

Article

A Model for Creep and Creep Damage in the γ -Titanium Aluminide Ti-45Al-2Mn-2Nb

William Harrison *, Zakaria Abdallah and Mark Whittaker

Materials Research Centre, Swansea University, Singleton Park, Swansea SA2 8PP, UK;

E-Mails: z.a.m.abdallah@swansea.ac.uk (Z.A.); m.t.whittaker@swansea.ac.uk (M.W.)

* Author to whom correspondence should be addressed; E-Mail: w.harrison@swansea.ac.uk;
Tel.: +44-1792-606-879; Fax: +44-1792-295-693.

Received: 6 January 2014; in revised form: 24 February 2014 / Accepted: 3 March 2014 /

Published: 14 March 2014

Abstract: Gamma titanium aluminides (γ -TiAl) display significantly improved high temperature mechanical properties over conventional titanium alloys. Due to their low densities, these alloys are increasingly becoming strong candidates to replace nickel-base superalloys in future gas turbine aeroengine components. To determine the safe operating life of such components, a good understanding of their creep properties is essential. Of particular importance to gas turbine component design is the ability to accurately predict the rate of accumulation of creep strain to ensure that excessive deformation does not occur during the component's service life and to quantify the effects of creep on fatigue life. The theta (θ) projection technique is an illustrative example of a creep curve method which has, in this paper, been utilised to accurately represent the creep behaviour of the γ -TiAl alloy Ti-45Al-2Mn-2Nb. Furthermore, a continuum damage approach based on the θ -projection method has also been used to represent tertiary creep damage and accurately predict creep rupture.

Keywords: gamma titanium aluminide; creep; intermetallics; θ -projection method

1. Introduction

The necessity to improve the efficiency of gas turbines drives research into materials suitable for applications at high temperatures. Furthermore, materials used in aeroengine components must have a high strength to weight ratio. Nickel-base superalloys are commonly used in gas turbine aeroengines,

particularly in the downstream turbine components, due to their superior mechanical properties at high temperatures as well as their considerable resistance to corrosion and oxidation. However, in comparison to conventional titanium alloys, nickel-base superalloys have a significantly higher density ($\cong 8.9 \text{ g}\cdot\text{cm}^{-3}$). In general, conventional titanium alloys are widely used in aeroengines due to their low densities ($\cong 4.5 \text{ g}\cdot\text{cm}^{-3}$) and their good mechanical properties at low temperatures. However, the creep resistance of such alloys is relatively inferior compared to the nickel-base superalloys in addition to their tendency to forming a brittle surface layer (α -case) at high temperatures [1]. Intermetallic gamma titanium aluminide (γ -TiAl) alloys encompass both the low density as well as the improved corrosion resistance properties compared to conventional titanium alloys, with significantly enhanced creep and oxidation resistance at high temperatures [2]. This makes them well suited for use in low pressure turbine (LPT) components as alternatives to the heavy nickel-base alloys. The service lives of these components are limited by the elevated stresses and temperatures under which they normally operate. Therefore, for safety critical components, it is imperative that one has a good understanding of the creep properties over a range of applied conditions.

Although it is important to understand the stress rupture behaviour of alloys, for aerospace applications it is essential to be able to predict the rate of accumulation of creep strain, not only to design against excessive deformation in a component, but also to quantify the effects of creep on fatigue life. Often creep rate is represented by a single value equal to the minimum creep rate, sometimes referred to as the “steady-state” creep and a number of methods have been proposed to relate this value to applied test conditions [3–5]. However, most alloys exhibit a constantly evolving creep rate where a minimum value is only observed for a short period of time “steady-state” creep is rarely perceived. Therefore, to accurately quantify the creep behaviour of a component for the duration of its life, a creep prediction method which accounts for the full shape of the creep curve from primary creep, through tertiary creep to rupture must be employed. The theta (θ) projection method [6,7] is an example of a convenient approach used to interpolate and extrapolate creep properties over a range of applied conditions. This method relates creep strain, ε , to time, t , using:

$$\varepsilon = \theta_1 \left(1 - e^{-\theta_2 t}\right) + \theta_3 \left(e^{\theta_4 t} - 1\right) \quad (1)$$

where θ_k ($k = 1-4$) are the 4- θ coefficients obtained from the experimental behaviour. This expression can be broken down into two parts, namely: primary creep represented by the expression $\theta_1 \left(1 - e^{-\theta_2 t}\right)$, where θ_1 is the magnitude of primary strain and θ_2 determines its rate of decay, and an accelerating creep rate due to tertiary effects represented by $\theta_3 \left(e^{\theta_4 t} - 1\right)$ with θ_3 scaling the tertiary creep strain and θ_4 determining its increase in rate. The coefficients θ_1 - and θ_3 are termed “scale” parameters whereas θ_2 and θ_4 are the “rate” parameters (Figure 1).

This method has been shown to accurately represent creep curves for a number of pure metals and alloys, e.g., copper [8], steels [9,10], titanium [11] and nickel-base superalloys [12–14], (Figure 2).

Figure 1. Creep curve showing primary, $\theta_1(1 - e^{-\theta_2 t})$, and tertiary, $\theta_3(e^{\theta_4 t} - 1)$, components.

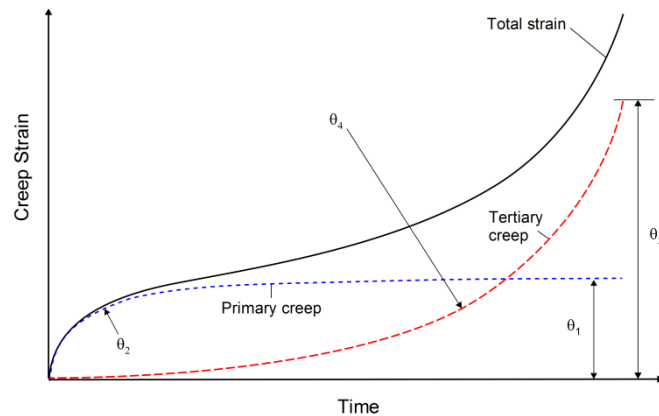
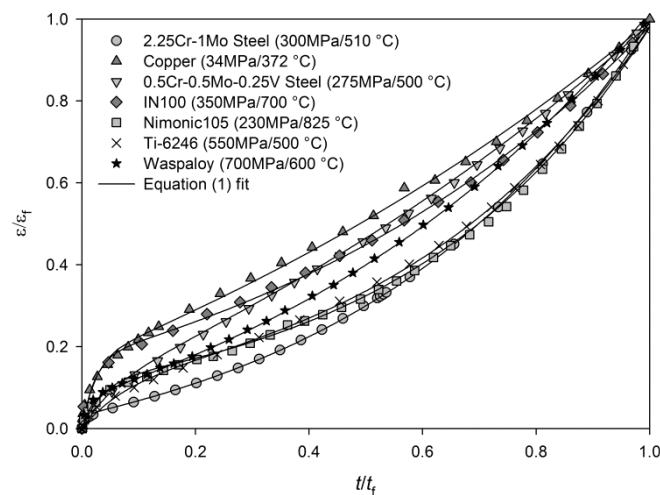


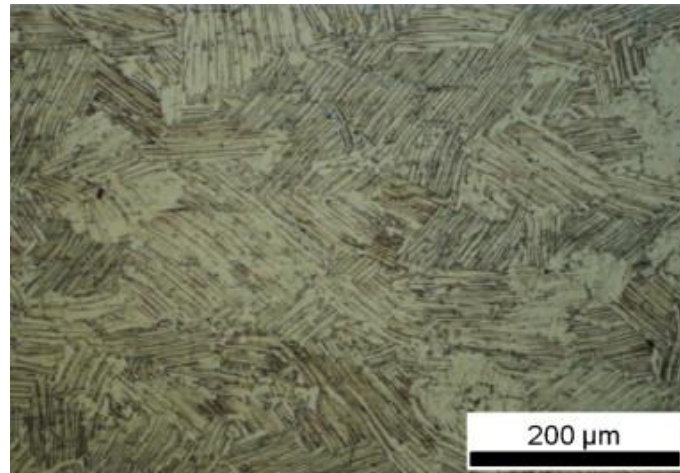
Figure 2. Examples of creep curves represented using Equation (1).



2. Experimental Data

Uniaxial constant-stress creep tests were performed in air according to ISO 204:2009 [15] on Ti-45Al-2Mn-2Nb specimens prepared from centrifugally cast and hot isostatically pressed (HIP) bar stocks. The alloy had been heat treated using a proprietary heat treatment to give a relatively coarse lamellar microstructure, Figure 3, consistent with previous studies [16,17].

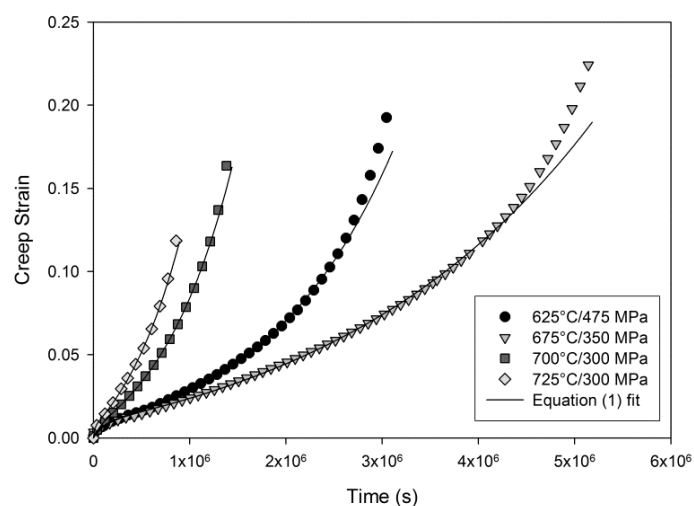
The test specimens had a diameter of 5.6 mm along the gauge section with a gauge length of 28 mm. In order to obtain a constant stress on the specimen throughout the duration of the test, the creep machines were equipped with an Andrade-Chalmers cam which compensates for the reduction of the gauge diameter during the course of each test. The testing temperatures ranged from 625 to 750 °C with applied stresses in the range of 150 to 550 MPa. The creep strain and temperature were, respectively, monitored using two high-precision linear variable differential transformers (LVDT) and calibrated type-R thermocouples.

Figure 3. Microstructure of the cast and HIP'ed Ti-45Al-2Mn-2Nb alloy.

3. Results

3.1. Creep Deformation

Normal creep curves were recorded for each test characterised by an initial strain on loading, ϵ_0 , followed by a period of primary creep where the rate of creep ($\dot{\epsilon} = d\epsilon/dt$) decreases to a minimum value, $\dot{\epsilon}_m$. Further creep deformation results in an increasing creep rate (tertiary creep) until failure (Figure 4). The rupture time and strain, t_f and ϵ_f respectively, were recorded and analysed in a previous study [18]. A ductile-like failure mode was observed on the fracture surfaces of all the tested specimens with pronounced necking, *i.e.*, reduction in area, within the gauge length. A set of θ coefficients have been obtained for each constant stress creep test. These are obtained by minimising the error between data points on experimentally obtained creep curves and values of strain calculated using Equation (1). The formation of a necked region prior to rupture indicates that failure was preceded by an area of mechanical inhomogeneity. This region is difficult to predict and once formed, local stress in this region will be higher than in the rest of the gauge length.

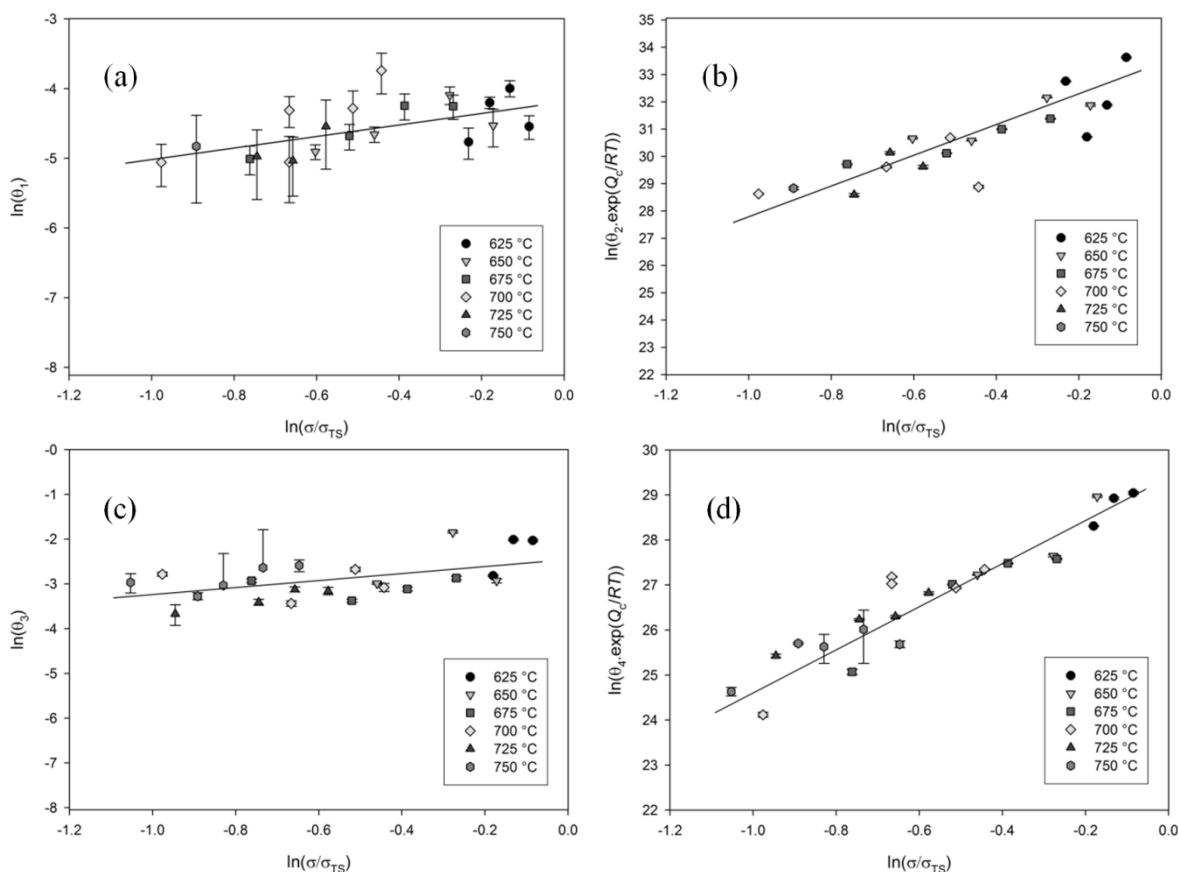
Figure 4. Ti-45Al-2Mn-2Nb creep curves with fits using Equation (1).

Therefore, when analysing constant stress creep curves, data points after the onset of necking must be ignored and the θ coefficients can accordingly be found by minimising the function ϕ^{n-l} of the form:

$$\phi^{n-l} = \sum_{i=1}^{n-l} \left\{ \epsilon_i - \theta_1 [1 - \exp(-\theta_2 t_i)] - \theta_3 [\exp(\theta_4 t_i) - 1] \right\}^2 \tag{2}$$

where the creep curve contains n displacement/time points, l is the onset of necking and ϵ_i is the experimental creep strain at time t_i . An iterative algorithm based on Newton’s method was used to find optimum values for θ which minimise ϕ^{n-l} with standard deviations calculated from the square root of the diagonal of the matrix of second order partial derivatives (the Hessian matrix). This is thoroughly investigated elsewhere [12] where the fitting process is discussed in more detail. The experimental data in Figure 4 are generally well represented taking into consideration the elimination of the last few points of each creep curve where inhomogeneity is likely to take place. The θ values obtained using this method are shown in Figure 5 with error bars showing \pm one standard deviation.

Figure 5. The dependence of: (a) θ_1 ; (b) θ_2 ; (c) θ_3 and (d) θ_4 with stress and temperature.



3.2. The Stress and Temperature Dependence of Creep

The θ coefficients obtained for each experimental curve are dependent on the applied stress and temperature. Figure 5 shows that θ_k , ($k = 1-4$), increases with either increase in stress and/or temperature. The θ coefficients can be related to the applied test conditions using a suitable function:

$$\theta_{k,h} = f(\sigma_h, T_h), k = 1, \dots, 4 \tag{3}$$

where $\theta_{k,h}$ are the coefficients obtained from h accelerated creep tests, with an applied stress and temperature of σ_h and T_h , respectively. For isotropic materials, a multi-linear function is often used:

$$\ln(\theta_k)_h = b_{k1} + b_{k2}\sigma_h + b_{k3}T_h + b_{k4}T_h\sigma_h, \quad k = 1, \dots, 4 \quad (4)$$

where b_{k1} to b_{k4} are material constants that are obtained from experimental data. However, Equation (4) has received criticism due to the fact that when $\sigma = 0$ and $T = 0$, $\theta_k = e^{b_{k1}}$ which illustrates that a creep rate will be predicted under zero stress and temperature. To overcome this problem, a power law type approach was used to interpolate the values of θ_{1-4} with respect to stress, σ , normalised by the ultimate tensile strength, σ_{TS} . The values of θ_1 and θ_3 showed little dependence on temperature when compared to the more pronounced dependence of θ_2 and θ_4 on temperature. Normalising σ by σ_{TS} is sufficient to account for temperature effects, since σ_{TS} is itself dependent on temperature. An Arrhenius expression has been employed to account for the effects of temperature in both primary and tertiary creep. Power law expressions have been used to relate the θ -coefficients to the normalised stress, σ/σ_{TS} according to:

$$\theta_1 = A_1 \left(\frac{\sigma}{\sigma_{TS}} \right)^{n_1} \quad (5)$$

$$\theta_2 = A_2 \left(\frac{\sigma}{\sigma_{TS}} \right)^{n_2} \exp\left(\frac{-Q_2^*}{RT}\right) \quad (6)$$

$$\theta_3 = A_3 \left(\frac{\sigma}{\sigma_{TS}} \right)^{n_3} \quad (7)$$

$$\theta_4 = A_4 \left(\frac{\sigma}{\sigma_{TS}} \right)^{n_4} \exp\left(\frac{-Q_4^*}{RT}\right) \quad (8)$$

where the stress exponents n_{1-4} and the scale factors A_{1-4} (Table 1) are derived from the experimentally obtained θ -coefficients, Q_2^* and Q_4^* are the activation energies for θ_2 and θ_4 and R is the universal gas constant ($8.314 \text{ J K}^{-1} \text{ mol}^{-1}$). An activation energy, Q_c^* , of $330 \text{ J K}^{-1} \text{ mol}^{-1}$ was found to be applicable when evaluating both θ_2 and θ_4 . It is worth noting that this value of activation energy, Q_c^* , is calculated at constant σ/σ_{TS} and is not equal to the activation energy for creep, Q_c , obtained by evaluating creep behaviour at constant stress, σ . n_1 and n_3 are obtained by calculating the gradient of the line which most accurately describes $\ln(\theta_1)$ against $\ln(\sigma/\sigma_{TS})$ and $\ln(\theta_3)$ against $\ln(\sigma/\sigma_{TS})$, respectively, using linear regression with $\ln(A_1)$ and $\ln(A_3)$ are equal to the y -intercepts. Similarly, n_2 and n_4 are obtained by calculating the gradient of the line which most accurately describes $\ln(\theta_2)\exp(-Q_c^*/RT)$ against $\ln(\sigma/\sigma_{TS})$ and $\ln(\theta_4)\exp(-Q_c^*/RT)$ against $\ln(\sigma/\sigma_{TS})$, respectively, with $\ln(A_2)$ and $\ln(A_4)$ equal to the y -intercepts. Plots of temperature compensated $\ln(\theta_{1-4})$ against $\ln(\sigma/\sigma_{TS})$ for Ti -45Al-2Mn-2Nb are shown in Figure 5a–d with linear trend lines.

Table 1. Values of A_k and n_k for Ti-45Al-2Mn-2Nb obtained from best fit lines in Figure 5.

k	A	n
1	0.016631	0.948228
2	1.8×10^{14}	4.940382
3	0.090096	0.883272
4	6.14×10^{12}	4.473413

Using the values of A_{1-4} and n_{1-4} in Table 1, creep curves for the Ti-45Al-2Mn-2Nb alloy at any specified testing condition can be reproduced (Figure 6). Confidence limits can be obtained creep curves for the θ -projection method by using the method described by Evans [12], however application of this technique is nontrivial. Instead, the accuracy of this method can be determined by comparing the calculated time to a pre-defined creep strain, t_ϵ , to those originally observed during testing. A good correlation between the predicted and the experimentally obtained values of time to 2% and 5% creep strain is prevalent in Figure 7a,b, respectively.

Figure 6. Ti-45Al-2Mn-2Nb creep curves with reproduced using Equations (5)–(8) and values of A_k and n_k in Table 1.

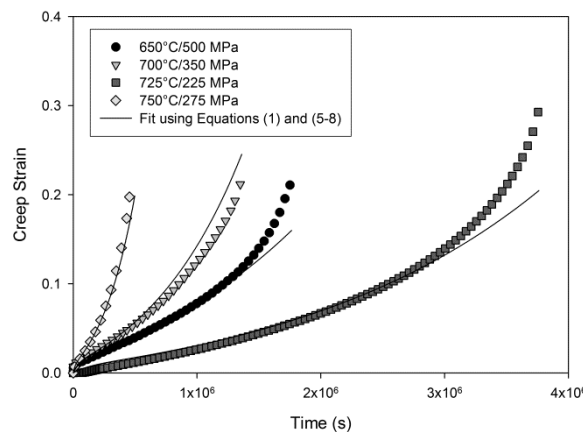
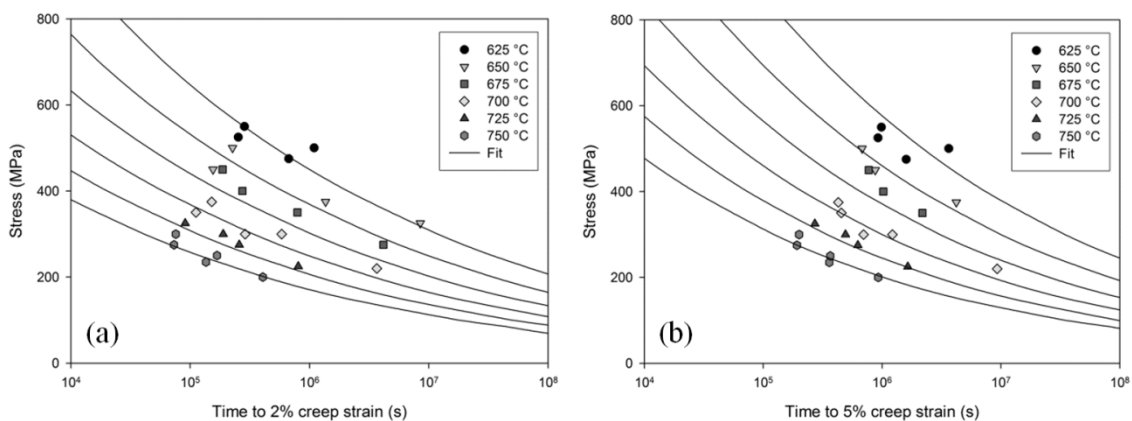


Figure 7. Calculated and experimental times to: (a) 2% and (b) 5% creep strain Ti-45Al-2Mn-2Nb using Equations (5)–(8) and values of A_k and n_k in Table 1.



3.3. Minimum Creep Rates

From Equation (1), it can be determined that the creep rate, $\dot{\epsilon}$, at any given time may be calculated using:

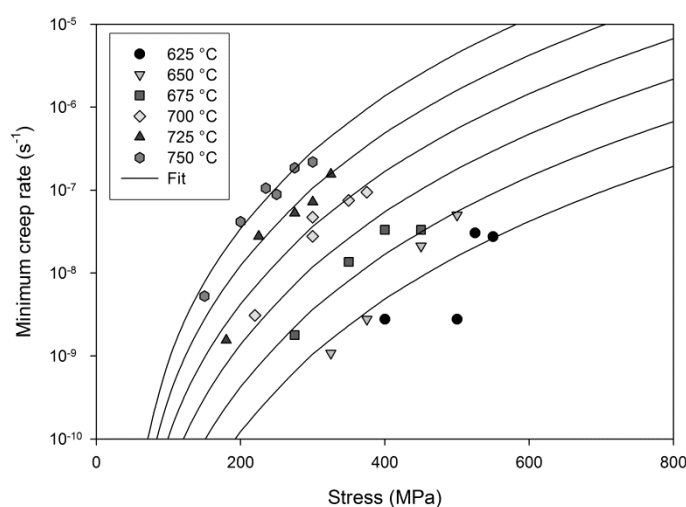
$$\dot{\epsilon} = \theta_1 \theta_2 \exp(-\theta_2 t) + \theta_3 \theta_4 \exp(-\theta_4 t) \quad (9)$$

Furthermore, the creep rate reaches a minimum value after time, t_m , which is given by:

$$t_m = \frac{1}{\theta_2 + \theta_4} \ln\left(\frac{\theta_1 \theta_2^2}{\theta_3 \theta_4^2}\right) \quad (10)$$

Therefore, the minimum creep rate, $\dot{\epsilon}_m$, can be calculated by substituting t_m into Equation (9). Using this method, with θ -values calculated using Equations (5)–(8), it is possible to predict $\dot{\epsilon}_m$ for a range of test conditions. These predicted values closely resemble those obtained experimentally. A comparison of predicted values for $\dot{\epsilon}_m$ and those observed experimentally is shown in Figure 8.

Figure 8. Minimum creep rates for Ti-45Al-2Mn-2Nb with predictions using Equations (5)–(10).



3.4. Stress Rupture

A phenomenological creep model has been derived based on the θ -projection method whereby creep rate is related to internal material state [14]. The basic formulation describes the evolution of creep rate based on state variables representing dislocation work hardening, internal softening and creep damage. For virgin material, these state variables are set to zero and their subsequent accumulation can be related to creep conditions using subsidiary equations [19] or by relation to the θ parameters [14]. Of particular interest when considering creep rupture is the accumulation of creep damage, represented by the damage parameter, W , which represents general long-range structure deterioration. Failure due to creep is assumed to occur when W reaches a critical value, W_{crit} , given by [20]:

$$W_{crit} = \frac{1}{\theta_3} \left[\epsilon_F - \theta_1 (1 - e^{-\theta_2 t_F}) \right] \quad (11)$$

where ϵ_F is the creep ductility obtained from creep tests and t_F is the measured stress rupture time. Values of W_{crit} obtained for Ti-45Al-2Mn-2Nb can be seen in Figure 9. W_{crit} is dependent on both

stress and temperature however, in a similar manner to the scale parameters, θ_1 and θ_3 , the effects of temperature can be compensated for by normalizing σ by σ_{TS} . The critical damage parameter, W_{crit} , can be related to test conditions using:

$$W_{crit} = c + \ln\left(\frac{\sigma}{\sigma_{TS}}\right)K \tag{12}$$

where K and c are material constants obtained by determining the gradient and y-intercept of W_{crit} against $\ln(\sigma/\sigma_{TS})$, respectively. For the Ti-45Al-2Mn-2Nb alloy, values of $K = -5.44$ and $c = 1.22$ were found. Since the rate of accumulation of creep damage, \dot{W} , can be described as:

$$\dot{W} = \theta_4 \exp(\theta_4 t) \tag{13}$$

rupture time, t_F , can be predicted when W/W_{crit} exceeds 1. Stress rupture times for the Ti-45Al-2Mn-2Nb alloy using this approach correlate well with the experimental measurements (Figure 10).

Figure 9. Relationship between W_{crit} and σ/σ_{TS} .

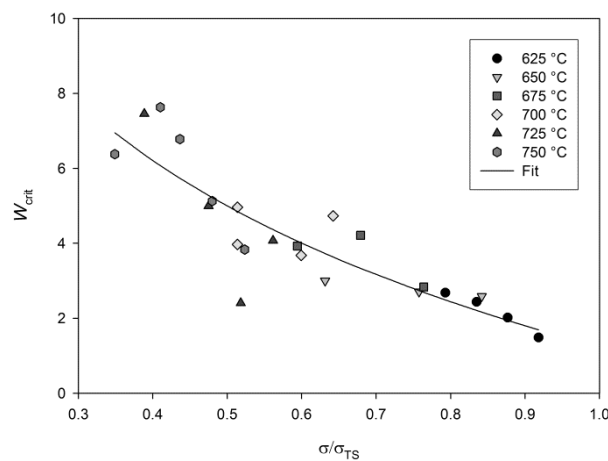
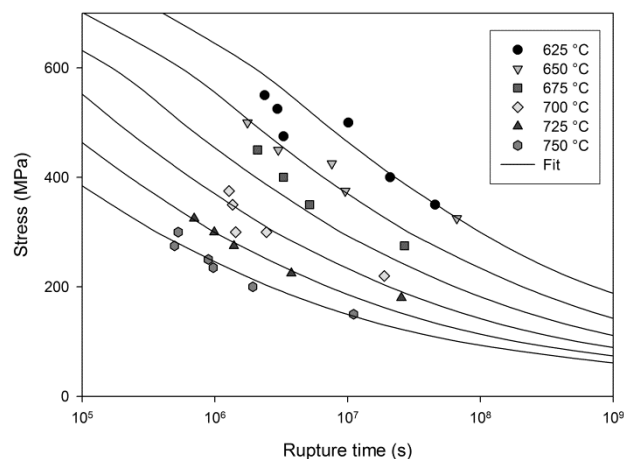
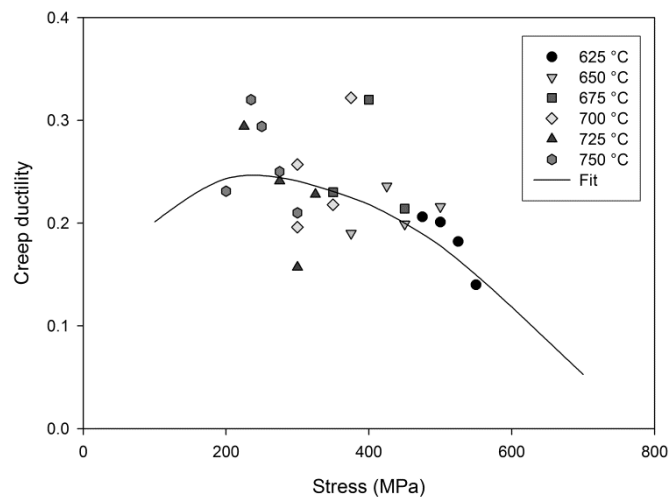


Figure 10. Stress rupture times for Ti-45Al-2Mn-2Nb with predictions when $W/W_{crit} > 1$.



Furthermore, the creep ductility can be calculated by substituting t_F into Equation (2). A characteristic of creep rupture at high temperatures is the high degree of scatter involved particularly with respect to failure strains [21]. The strains at failure recorded for this Ti-45Al-2Mn-2Nb alloy display a large variability with strains of between 13% and 34% being recorded at rupture. Creep ductilities can be calculated by determining the value of ϵ when $W/W_{crit} > 1$. A comparison of the calculated and experimentally obtained creep ductilities for the Ti-45Al-2Mn-2Nb alloy is shown in Figure 11.

Figure 11. Creep ductility at failure for Ti-45Al-2Mn-2Nb with predictions when $W/W_{crit} > 1$.



4. Discussion

Given the relatively low levels values of standard error shown in Figure 5a–d, Equation (2) has represented the experimental creep curves of the Ti-45Al-2Mn-2Nb alloy well. The higher levels of errors observed when evaluating θ_1 are due to the stochastic nature of primary creep and are often observed when this method is employed using this method [14]. Attempts have been made in the past to reduce such errors by adding an additional primary creep term to Equation (2) [22]. The θ -coefficients obtained by minimising the function given in Equation (2) are dependent on both stress and temperature (Figure 5). The rate parameters θ_2 and θ_4 exhibit a much greater dependence on both stress and temperature when compared to the scale parameters θ_1 and θ_3 . The stress exponents of parameters θ_1 and θ_3 are both less than unity whereas those for the rate parameters θ_2 and θ_4 , represented by the slopes of the plots in Figure 5b,d, are close to 5, which is consistent with the stress exponent observed for stress rupture for a number of alloys [23]. However, the values of A_{1-4} and n_{1-4} obtained in this study are only relevant for the alloy investigated since the creep rates of titanium aluminides are strongly dependent on microstructure [24]. Since the parameters θ_1 and θ_3 display little dependence on temperature, normalising the applied stress, σ , by σ_{TS} at each creep temperature is sufficient to collapse all the data points on to a single master curve. However, θ_2 and θ_4 exhibit a much greater dependence on temperature and an Arrhenius expression is used to collapse the θ coefficients on to a single curve.

An activation energy, $Q_C^* = 330 \text{ K J mol}^{-1}$, was found to well represent both primary creep, represented by θ_2 , and tertiary creep, represented by θ_4 , in Ti-45Al-2Mn-2Nb. This value is consistent

with that observed by Abdallah *et al.* for creep rupture [18]. Previous studies have found that the activation energy, Q_C , falls within the range 300 to 440 K J mol⁻¹ for a range of γ -TiAl and fully lamellar TiAl alloys with an average value of 375 K J mol⁻¹ [25,26]. However, these values of Q_C are evaluated under constant stress. Since ultimate tensile strength, σ_{TS} , decreases with increasing temperature, the value of Q_C^* evaluated against σ/σ_{TS} in this study is lower than Q_C . It is interesting to note that the value of Q_C^* found in this study is slightly higher than the activation energy for titanium self-diffusion in the γ -TiAl alloy (291 K J mol⁻¹) which occurs via a vacancy mechanism [27], but the same as the measured interdiffusion coefficient for γ -TiAl [26] indicating that interdiffusion has an important role in the creep of Ti-45Al-2Mn-2Nb. The creep properties of some creep resistant alloys, such as the nickel-based superalloy Waspaloy [28], bainitic [29] and austenitic [30] steels exhibit transitions in activation energy with different applied test conditions. These changes are attributed to different micro-mechanism, whether inferred or observed. Ashby [31] maps have been used to describe the transitions in mechanism between different applied conditions for a range of pure metals and alloys. Ashby describes two main categories of deformation relevant to creep, dislocation based and diffusion based. More recent studies cast doubt on the role of pure diffusion in the creep of alloys under operational conditions, attributing deformation different diffusion controlled dislocation mechanisms [32]. The creep properties of other alloys, such as the titanium alloys Ti6-4 [33] and Ti-834 [34] display a constant activation energy across all test conditions despite a variation in stress dependence, denoted by a transition in stress exponent. This has, in part, been attributed to the low rates of work hardening in titanium. The values of the constants n_{1-4} and Q_C^* across all test conditions in Ti-45Al-2Mn-2Nb infer that the mechanism of creep remains the same. Justification for this can be found in the lamellar microstructure of the alloy which constrains dislocation movement. Studies [25] of other lamellar γ -TiAl alloys have identified dislocation climb as the rate determining process at stresses above about 200 MPa. These studies have focused mainly on single property predictions of minimum creep rate or stress rupture life. Of particular interest in this study is the evolution of creep mechanism through the duration of a creep test from primary to tertiary creep. Primary creep in lamellar TiAl alloys has been attributed to the movement of dislocations formed at high stress lamellar interfaces [35], whereas tertiary creep has been attributed to the formation of microvoids caused by the strain incompatibilities between lamellar grains [36]. Despite different mechanisms being responsible for primary and tertiary creep, both are driven by diffusion controlled dislocation movement within the constraints of the lamellar microstructure and as such a single activation energy, Q_C^* , based on interdiffusion can be used for both Equations (6) and (8).

A number of creep life assessment methods exist, such as the traditional Norton's power law [3], the Larson-Miller parameter [37] and the more recent methods such as the hyperbolic tangent [5] and the Wilshire Equations [32] methods, have shown to extrapolate creep properties across a range of test conditions with varying degrees of success. A detailed assessment of the application of these creep life methods to the Ti-45Al-2Mn-2Nb alloy has been performed by Abdallah *et al.* [18]. However, these methods do not account for the full shape of the creep curve and the evolution of creep rate with time. The times to strain, minimum creep rates and stress rupture lives predicted using the method described in this paper represent the experimental data well across a range of test conditions. This allows confidence in the method to predict creep properties at untested conditions, allowing the method to be used in finite element analyses of components in which the stress and/or temperature

vary. One criticism of methods, such as the one presented in this paper, is that at values of applied stress greater than the σ_{TS} of the material, predictions of finite creep rates and rupture lives were observed in excess of those obtained experimentally. In reality, as $\sigma \rightarrow \sigma_{TS}$, $\dot{\epsilon} \rightarrow \infty$ and $t_F \rightarrow 0$, however, the mechanism of failure at stresses close to σ_{TS} is not purely a creep mechanism. Furthermore, during component analyses, regions of high stress will quickly relax due to the inelastic effects of creep and plasticity.

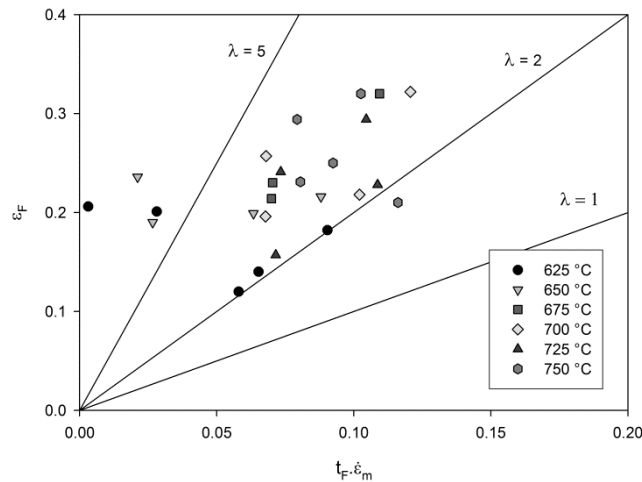
An advantage of the θ - projection technique is that the creep rate can be related to internal material state variables [14]. This approach provides better predictions of the creep rate when changes in the applied stress and temperature occur during creep, compared to time or strain hardening models [38]. Furthermore, evaluation of the damage parameter, W , allows a more phenomenological approach to predicting creep rupture than purely empirical methods. Since the rate of accumulation of W is dependent on θ_4 , it is assumed that primary creep processes have no effect on rupture. Since the formation of microvoids between lamellar grains has been identified as the damage mechanism of tertiary creep, W can be assumed to represent this mechanism. The rate of accumulation of damage, W , determined by θ_4 , can be calculated using Equation (8) and so comparing the parameters A_4 and n_4 obtained for different variant of γ -TiAl will help to characterise the alloys damage tolerance. Final rupture occurs when the creep damage becomes sufficient that the specimen fails under the applied load. The critical damage, W_{crit} , is therefore dependent on applied stress as shown in Figure 9. Creep rupture times predicted as $W/W_{crit} > 1$ represent the experimental data well and creep ductilities predicted using this damage approach fail within experimentally observed elongations at failure however there is considerable scatter in the observations. Ductilities of between 13% and 34% were observed, which are considerably more than tensile ductilities observed at ambient temperature (1%–2%). The model predicts a maximum ductility of 25% at approx. 250 MPa. This prediction is dependent on both the rate of accumulation of W and the magnitude of W_{crit} . As stress increases above 250 MPa, W_{crit} decreases more significantly than the rate of accumulation of W with respect to ϵ . Below this stress, internal creep damage, represented by W accumulates more rapidly with respect ϵ and therefore rupture is predicted at a lower ϵ despite W_{crit} having a greater magnitude. An indication of the damage processes preceding tertiary creep can be obtained by evaluating the creep damage tolerance parameter, λ , for all test conditions where:

$$\lambda = \epsilon_t / \dot{\epsilon}_m t_f \quad (14)$$

where ϵ_t is the tertiary creep strain [39]. Wilshire *et al.* [40] have shown that metals and alloys which have stable microstructures despite the presence of several damage mechanisms, such as intergranular or transgranular cracking, display a damage tolerance parameter, $\lambda < 2$. However, $\lambda > 2$ is observed for alloys where tertiary creep initiates due to microstructural instability. For the Ti-45Al-2Mn-2Nb alloy, the value of λ was greater than 2 for all the investigated test conditions, with the exception of few tests exhibiting $\lambda > 5$ (Figure 12) giving an indication of a progressive loss of creep strength due to some microstructural instability during tertiary creep. These tests were conducted at relatively high stress indicating that some translamellar cracking could have occurred with subsequent reduction in creep strength. An analysis of the creep failure of Ti-45Al-2Mn-2Nb tensile specimens has been performed by Abdallah *et al.* [18]. This study identifies relatively flat fracture planes and a significant

reduction in cross-sectional area. Interlamellar and intergranular cracking were observed in the region of the fracture surface with subsidiary surface cracking but no surface oxidation.

Figure 12. Relationship between ε_f and $\dot{\varepsilon}_m \cdot t_f$.



5. Conclusions

The theta (θ) projection method provides a good representation of the creep behaviour of the intermetallic gamma titanium aluminide Ti-45Al-2Mn-2Nb over a range of test conditions. A power law type relationship has been used to relate the θ -coefficients to the applied stress with a stress exponent close to unity for θ_1 and θ_3 in comparison to a stress exponent of about 5 for θ_2 and θ_4 . An Arrhenius expression has been employed to account for temperature with the activation energy, Q_C^* , evaluated against σ/σ_{TS} . For θ_2 and θ_4 , an activation energy of $Q_C^* = 330 \text{ K J mol}^{-1}$ which correlates to observed micromechanical processes was obtained. Predicted times to pre-defined strain levels using this approach correlated well with the test data providing well-represented minimum creep rate values. The stress rupture times and creep ductility were successfully predicted using an internal damage approach which well represented the actual measurements. An analysis of the shapes of the creep curve showed that the loss of creep strength during the tertiary creep is due to some microstructural instability.

Acknowledgments

This research was carried out as part of a strategic partnership between Swansea University, the Engineering and Physical Sciences Research Council (EPSRC) and Rolls-Royce plc. The financial support from EPSRC and Rolls-Royce plc is greatly appreciated.

Author Contributions

The work presented here was carried out as a collaboration between all authors. The research theme was defined by William Harrison, Zakaria Abdallah and Mark Whittaker. Zakaria Abdallah carried out the mechanical testing and subsequent failure analysis. William Harrison analysed the data, performed the numerical analysis and wrote the paper. William Harrison and Mark Whittaker co-worked on the

discussion and interpreted the numerical observations with respect to micromechanical behaviour. All authors have contributed to, seen and approved the manuscript.

Conflicts of Interest

The authors declare no conflict of interest.

References

1. Evans, R.W.; Hull, R.J.; Wilshire, B. The effects of alpha-case formation on the creep fracture properties of the high-temperature titanium alloy IMI834. *J. Mater. Process. Technol.* **1996**, *56*, 492–501.
2. Loria, E.A. Quo vadis gamma titanium aluminide. *Intermetallics* **2001**, *9*, 997–1001.
3. Norton, F.H. *The Creep of Steel at High Temperatures*; McGraw-Hill Book Company: New York, NY, USA, 1929.
4. Dorn, J.E. Some fundamental experiments on high temperature creep. *J. Mech. Phys. Solids* **1955**, *3*, 85–116.
5. McVetty, P.G. Creep of metals at elevated temperatures: The hyperbolic sine relation between stress and creep rate. *ASME Trans.* **1943**, *65*, 761–769.
6. Evans, R.W.; Parker, J.D.; Wilshire, B. An extrapolation procedure for long-term creep strain and creep life prediction with special reference to 0.5Cr0.5Mo0.25V ferritic steels. In Proceedings of the Recent Advances in Creep and Fracture of Engineering Materials and Structures, Swansea, UK, 24–27 March 1981.
7. Evans, R.W.; Wilshire, B. *Creep of Metals and Alloys*; The Institute of Metals: London, UK, 1985; pp. 197–243.
8. Brown, S.G.R.; Evans, R.W.; Wilshire, B. New approach to creep of pure metals with special reference to polycrystalline copper. *Mater. Sci. Technol.* **1987**, *3*, 23–27.
9. Evans, R.W.; Parker, J.D.; Wilshire, B. The θ projection concept—A model-based approach to design and life extension of engineering plant. *Int. J. Press. Vessel. Pip.* **1992**, *50*, 147–160.
10. Brown, S.G.R.; Evans, R.W.; Wilshire, B. Exponential descriptions of normal creep curves. *Scr. Metall.* **1986**, *20*, 855–860.
11. Evans, R.W.; Beden, I.; Wilshire, B. Creep life prediction for 0.5Cr0.5Mo0.25V ferritic steel. In Proceedings of the 2nd International Conference on Creep and Fracture of Engineering Materials and Structures, Swansea, UK, 1–6 April 1984.
12. Evans, R.W. Statistical scatter and variability of creep property estimates in θ projection method. *Mater. Sci. Technol.* **1989**, *5*, 699–707.
13. Girdwood, R.B.; Evans, R.W. Recovery of creep properties of the nickel-base superalloy nimonic 105. *Int. J. Press. Vessel. Pip.* **1996**, *66*, 141–153.
14. Evans, R.W. A constitutive model for the high-temperature creep of particle-hardened alloys based on the θ projection method. *Proc. R. Soc. A Math. Phys. Eng. Sci.* **2000**, *456*, 835–868.
15. International Organization for Standardization (ISO). *Metallic materials—Uniaxial creep testing in tension—Method of test*; ISO 204:2009; ISO: Geneva, Switzerland, 2009.

16. Prasad, U.; Chaturvedi, M. Influence of alloying elements on the kinetics of massive transformation in gamma titanium aluminides. *Metall. Mater. Trans. A* **2003**, *34*, 2053–2066.
17. Diologent, F.; Kruml, T. Measurement of the effective activation volume in 45XD titanium aluminides by repeated transient tests. *Mater. Sci. Eng. A* **2008**, *487*, 377–382.
18. Abdallah, Z.; Whittaker, M.T.; Bache, M.R. High temperature creep behaviour in the γ titanium aluminide Ti-45Al-2Mn-2Nb. *Intermetallics* **2013**, *38*, 55–62.
19. Evans, R.W.; Evans, M. Numerical modelling of small disc creep test. *Mater. Sci. Technol.* **2006**, *22*, 1155–1162.
20. Evans, R.W.; Wilshire, B. Constitutive Laws for High Temperature Creep and Fracture. In *Unified Laws of Plastic Deformation*; Krausz, A.S., Krausz, K., Eds.; Academic Press: London, UK, 1996; pp. 107–152.
21. Guest, J.C. Standards in Elevated Temperature Tensile and Uniaxial Creep Testing. In *Measurement of High Temperature Mechanical Properties of Materials*; Loveday, M.S., Day, M.F., Dyson, B.F., Eds.; HMSO: London, UK, 1982; pp. 23–31.
22. Evans, M. Predicting times to low strain for a 1CrMoV rotor steel using a 6- θ projection technique. *J. Mater. Sci.* **2000**, *35*, 2937–2948.
23. Daehn, G.S.; Brehm, H.; Lee, H.; Lim, B.-S. A model for creep based on microstructural length scale evolution. *Mater. Sci. Eng. A* **2004**, *387–389*, 576–584.
24. Zhang, W.J.; Deevi, S.C. Analysis of the minimum creep rates of TiAl alloys. *Mater. Sci. Eng. A* **2003**, *362*, 280–291.
25. Beddoes, J.; Wallace, W.; Zhao, L. Current understanding of creep behaviour of near γ -titanium aluminides. *Int. Mater. Rev.* **1995**, *40*, 197–217.
26. Parthasarathy, T.A.; Mendiratta, M.G.; Dimiduk, D.M. Observations on the creep behavior of fully-lamellar polycrystalline TiAl: Identification of critical effects. *Scr. Mater.* **1997**, *37*, 315–321.
27. Kroll, S.; Mehrer, H.; Stolwijk, N.; Herzig, C.; Rosenkranz, R.; Frommeyer, G. Titanium self-diffusion in the intermetallic compound γ -TiAl. *Z. Metallkd.* **1992**, *83*, 591–595.
28. Wu, X.; Williams, S.; Gong, D. A true-stress creep model based on deformation mechanisms for polycrystalline materials. *J. Mater. Eng. Perform.* **2012**, *21*, 2255–2262.
29. Whittaker, M.T.; Wilshire, B. Creep and creep fracture of 2.25Cr–1.6W steels (Grade 23). *Mater. Sci. Eng. A* **2010**, *527*, 4932–4938.
30. Whittaker, M.T.; Evans, M.; Wilshire, B. Long-term creep data prediction for type 316H stainless steel. *Mater. Sci. Eng. A* **2012**, *552*, 145–150.
31. Ashby, M.F. A first report on deformation-mechanism maps. *Acta Metall.* **1972**, *20*, 887–897.
32. Wilshire, B.; Battenbough, A.J. Creep and creep fracture of polycrystalline copper. *Mater. Sci. Eng. A* **2007**, *443*, 156–166.
33. Whittaker, M.T.; Harrison, W.J.; Lancaster, R.J.; Williams, S. An analysis of modern creep lifing methodologies in the titanium alloy Ti6–4. *Mater. Sci. Eng. A* **2013**, *577*, 114–119.
34. Abdallah, Z.; Perkins, K.; Williams, S. Advances in the Wilshire extrapolation technique—Full creep curve representation for the aerospace alloy titanium 834. *Mater. Sci. Eng. A* **2012**, *570*, 176–182.
35. Beddoes, J.; Seoa, D.Y.; Chenb, W.R.; Zhaob, L. Relationship between tensile and primary creep properties of near γ -TiAl intermetallics. *Intermetallics* **2001**, *9*, 915–922.

36. Beddoes, J.; Zhao, L.; Au, P.; Dudzinsky, D.; Triantafillou, J. *Structural Intermetallics 1997*; Nathal, M.V., Darolia, R., Liu, C.T., Martin, P.L., Miracle, D.B., Wagner, R., Yamaguchi, M., Eds.; TMS: Warrendale, PA, USA, 1997.
37. Larson, F.R.; Miller, E.J. Time-temperature relationship for rupture and creep stresses. *ASME Trans.* **1952**, *74*, 765–775.
38. Harrison, W.J.; Whittaker, M.T.; Deen, C. Creep behaviour of Waspaloy under non-constant stress and temperature. *Mater. Res. Innov.* **2013**, *17*, 323–326.
39. Leckie, F.A.; Hayhurst, D.R. Constitutive equations for creep rupture. *Acta Metall.* **1977**, *25*, 1059–1070.
40. Wilshire, B.; Burt, H. Tertiary creep of metals and alloys. *Z. Metallkd.* **2005**, *96*, 552–557.

© 2014 by the authors; licensee MDPI, Basel, Switzerland. This article is an open access article distributed under the terms and conditions of the Creative Commons Attribution license (<http://creativecommons.org/licenses/by/3.0/>).